Performance metrics for Fourier drag models in low Earth orbit determination and prediction

Vishal Ray
University of Colorado Boulder
Daniel J. Scheeres
University of Colorado Boulder

ABSTRACT

Fourier drag-coefficient models allow higher-order attitude and orbit-dependent frequencies present in the drag-coefficient to be estimated during the orbit determination process. In order to obtain the best possible orbit determination performance, an observable set of Fourier coefficients needs to be selected for estimation. An observability analysis combining various existing metrics is performed in order to conclusively determine an estimation set for the different Fourier drag-coefficient models. The observability analysis results are directly compared with the orbit determination performance in terms of traditional performance metrics. It is demonstrated that a better orbit fit may not always lead to a better orbit prediction. A new performance metric, integrated acceleration error, is introduced to better gauge the prediction performance.

1. INTRODUCTION

The modeling of drag-coefficients has received attention in the past two decades because of its importance in both orbit determination and prediction of satellite orbits as well as inversion of atmospheric densities from orbit decay data. Whereas earlier, the drag-coefficient was primarily modeled using a cannonball model [1], i.e., considered constant in most applications, recent advances in physics-based modeling have allowed a time-varying representation of the drag-coefficient. In a set of previous papers, the authors proposed Fourier drag-coefficient models that capture specific frequencies of the time-varying drag-coefficient in an estimation framework [2, 3]. It was demonstrated that supplementing the cannonball estimate (Order 0) with higher-order Fourier coefficient estimates that govern orbit-dependent and attitude-dependent frequencies can improve orbit determination and prediction significantly. A body-fixed Fourier (BFF) model was developed to capture attitude-dependence of the drag-coefficient while an orbit-fixed Fourier (OFF) model was developed because of the orbit-dependence of the drag-coefficient. The overall dependence of the drag-coefficient on both attitude and orbit-related factors was modeled with body-orbit double Fourier (BODF) and body-orbit summation (BOS) methods. In this paper, a framework is developed to evaluate the performance of the Fourier models in orbit determination and prediction. The performance of higher-fidelity models such as the Fourier models is usually evaluated based on the accuracy of the orbit fit and the improvements in the orbit prediction into the future. The common performance metrics used for this purpose are 1. post-fit residuals - the error between the actual measurements and filter-predicted measurements, 2. estimation error in initial states - the error between the estimated initial states and true initial states and error in the estimated parameter such as the effective drag-coefficient. This work demonstrates that an improved orbit determination as evaluated using the given performance metrics does not necessarily lead to an improved orbit prediction, even in the absence of any other unmodeled dynamics. In this context, a new performance metric is proposed - the integrated acceleration error – that is more strongly correlated with the orbit prediction than any of the other metrics.

The performance of a multiple-parameter model in estimation theory is strongly dependent on the observability of its parameters. Observability analysis of a system forms an integral part of determining what parameters can be estimated with the given information. There are two aspects to the effects of parameters on a system. First, whether a parameter has a non-zero effect on the dynamics distinct from the effects of other parameters. Second, if the effects remain distinguishable when translated to the measurement space. Observability analysis deals with the latter. Observability of a system has been extensively explored in aerospace engineering systems through various observability matrix metrics.

The commonly used binary test for observability based on the rank of the observability matrix is defined for linear systems but can be extended to linearized systems such as the orbit determination problem here. There are multiple other measures of observability that can be utilized to understand the extent or degree to which a parameter is observable. The degree of observability can be determined by how close the observability matrix is to singularity through measures such as condition number of the observability matrix [4, 5, 6], singular values of the observability matrix [6, 7] and the cost function of the optimization algorithm [8]. Metrics such as the correlation coefficient can be utilized to remove sets of highly correlated parameters [9] whose effects on the measurements might be indistinguishable.

Even though these measures quantify the observability of the system, they don't provide a direct method to determine which states and parameters are observable. All the metrics can be evaluated by removing combinations of parameters from the estimation subset and then comparing the metric values to determine which parameters are poorly observable. But it can become quite cumbersome for systems with a large number of parameters. The concept of parameter identifiability [10], frequently encountered in environmental and biological systems, is useful in determining what parameter subset should be estimated. Instead of deducing observability directly, the parameters can be ranked based on sensitivity of the measurements to the parameters. Using orthogonalization methods on the measurement sensitivity matrix allows a ranking of the parameters based on the norm of the sensitivity as well as the linear dependence of the sensitivity vectors [11, 12, 13].

The observability of a system is intricately tied to the uncertainties of the estimated coefficients. Adding more parameters to the estimation subset increases uncertainties of the estimated coefficients with a given data-arc according to the Information Dilution Theorem [14]. On the other hand, ignoring parameters with large distinct effects on the measurements can lead to filter divergence where the uncertainties of the estimated coefficients are small but the estimated errors are large due to aliasing effects [15]. A consider covariance analysis can reveal the coefficients, ignoring which will have negligible effect on the uncertainties of the estimated coefficients [16]. In this work, different observability metrics are used in combination with parameter-ranking methods based on measurement sensitivities and consider covariance analysis to conclusively determine which Fourier coefficients need to be estimated for different cases.

The paper is organized as follows. The Fourier coefficient models are discussed in section 2. Section 3 discusses the observability metrics that are used to determine the estimation subset of the Fourier coefficients as well as the performance metric that is used to analyze the prediction performance. The application of the observability methods to synthetic data with direct comparison to orbit determination performance using Monte Carlo simulations is discussed in section 4. The results of the prediction performance in terms of the integrated acceleration error are discussed in section 5. Section 6 states the key conclusions of the paper.

2. FOURIER DRAG-COEFFICIENT MODELS

This section provides details of the Fourier drag-coefficient models used in the estimator. The reader is referred to Ray et al. [2] for the details of incorporating the models in an estimation framework.

2.1 Orbit-fixed Fourier model

The drag-coefficient varies with ambient parameters such as the partial pressure of atomic oxygen, atmospheric composition and ambient temperature. Under the assumptions of a symmetric exponentially decaying atmosphere, the atmospheric composition and partial pressure of oxygen are both periodic in the orbit since they are functions of only altitude in this case while the ambient temperature is constant. The drag-coefficient is also a function of the velocity of the satellite that is periodic as well. Even in the case of a realistic atmosphere, the variations in orbit are quasi-periodic. Therefore, the drag-coefficient can be expressed as a Fourier series expansion around the eccentric anomaly (E) in the orbit frame of the satellite as follows

$$C_D = \sum_{n=0}^{\infty} (\overline{\mathbb{A}}_n \cos nE + \overline{\mathbb{B}}_n \sin nE). \tag{1}$$

where $\overline{\mathbb{A}}_n$ and $\overline{\mathbb{B}}_n$ are Fourier coefficients that are calculated by integrating the drag coefficient over one period as follows

$$\overline{\mathbb{A}}_n = \frac{1}{\pi} \int_0^{2\pi} C_D \cos nE dE, \tag{2}$$

$$\overline{\mathbb{B}}_n = \frac{1}{\pi} \int_0^{2\pi} C_D \sin nE dE, \tag{3}$$

for $n > 0$ and,

$$\overline{\mathbb{A}}_0 = \frac{1}{2\pi}\int_0^{2\pi} C_D dE, \tag{4}$$

for $n = 0$. Any drag-coefficient model can be parameterized in this manner by numerically evaluating the integrals given by Eqs. 14-17.

2.2 Body-fixed Fourier model

If the velocity vector rotates around a single axis in the body frame of the satellite, then the drag-coefficient can be expanded as a Fourier series around the angle of rotation (θ) as

$$C_D = \sum_{n=0}^{\infty} (\overline{\mathscr{A}}_n \cos n\theta + \overline{\mathscr{B}}_n \sin n\theta). \tag{5}$$

where the coefficients are given by,

$$\overline{\mathscr{A}}_n = \frac{1}{\pi}\int_0^{2\pi} C_D \cos n\theta d\theta, \tag{6}$$

$$\overline{\mathscr{B}}_n = \frac{1}{\pi}\int_0^{2\pi} C_D \sin n\theta d\theta, \tag{7}$$

for $n > 0$ and,

$$\overline{\mathscr{A}}_0 = \frac{1}{2\pi}\int_0^{2\pi} C_D d\theta, \tag{8}$$

and $\overline{\mathscr{B}}_0 = 0$ for $n = 0$. The integration can be carried out numerically in order to compute initial estimates of the coefficients. To calculate the integrals, a GSIM is selected for C_D along with a shape model for the satellite. The drag-coefficient model doesn't necessarily have to be analytical. For example, direct simulation Monte Carlo (DSMC) [17] can be used to compute the drag-coefficient for varying θ and the resultant drag-coefficient profile can be parameterized in the Fourier series. Alternatively, for simple shapes, the satellite can be assumed to comprise of multiple flat plates and the analytical drag-coefficients of individual plates can be summed up to arrive at the total drag-coefficient for the satellite [18]. The resultant drag-coefficients of the satellite can then be integrated over the angle of variation of the velocity vector in the body frame using Eqs. 14 and 15 to compute the initial estimates of the Fourier coefficients.

2.3 Body-orbit double Fourier (BODF) model

In developing the theory for the BFF model, the Fourier coefficients were assumed to be constant in the orbit. But since the drag-coefficient is a function of ambient parameters, the body-fixed Fourier coefficients are periodic functions of the eccentric anomaly. This allows the body-fixed Fourier coefficients to be expressed as Fourier series expansions around the eccentric anomaly.

$$\overline{\mathscr{A}}_n(E) = \sum_{m=0}^{\infty} (\overline{\mathbb{A}}_{mn} \cos mE + \overline{\mathbb{B}}_{mn} \sin mE), \tag{9}$$

$$\overline{\mathscr{B}}_n(E) = \sum_{m=0}^{\infty} (\overline{\mathbb{C}}_{mn} \cos mE + \overline{\mathbb{D}}_{mn} \sin mE). \tag{10}$$

Therefore, the total drag-coefficient can be expressed as a body-orbit double Fourier (BODF) model [3],

$$\begin{aligned} C_d = \sum_{m=0}^{\infty}\sum_{n=0}^{\infty} (&\overline{\mathbb{A}}_{mn} \cos mE \cos n\phi + \overline{\mathbb{B}}_{mn} \sin mE \cos n\phi \\ &+ \overline{\mathbb{C}}_{mn} \cos mE \sin n\phi + \overline{\mathbb{D}}_{mn} \sin mE \sin n\phi). \end{aligned} \tag{11}$$

The BODF coefficients can be obtained by carrying out a Fourier expansion of the analytical BFF coefficients obtained in the previous section as follows

$$\overline{\mathbb{A}}_{mn} = \frac{1}{\pi}\int_0^{2\pi} \overline{\mathscr{A}}_n(E) \cos mE dE, \tag{12}$$

$$\overline{\mathbb{B}}_{mn} = \frac{1}{\pi}\int_0^{2\pi} \overline{\mathscr{A}}_n(E) \sin mE dE, \tag{13}$$

$$\overline{\mathbb{C}}_{mn} = \frac{1}{\pi}\int_0^{2\pi} \overline{\mathscr{B}}_n(E)\cos mE dE, \tag{14}$$

$$\overline{\mathbb{D}}_{mn} = \frac{1}{\pi}\int_0^{2\pi} \overline{\mathscr{B}}_n(E)\sin mE dE, \tag{15}$$

for $m > 0$ and,

$$\overline{\mathbb{A}}_{0n} = \frac{1}{2\pi}\int_0^{2\pi} \overline{\mathscr{A}}_n(E) dE, \tag{16}$$

$$\overline{\mathbb{C}}_{0n} = \frac{1}{2\pi}\int_0^{2\pi} \overline{\mathscr{B}}_n(E) dE, \tag{17}$$

and $\overline{\mathbb{B}}_{0n} = 0$, $\overline{\mathbb{D}}_{0n} = 0$ for $m = 0$. If the coupled coefficients with $m \neq 0, n \neq 0$ are ignored, then the BODF model reduces to a body-orbit summation (BOS) model that is a sum of BFF and OFF models.

3. OBSERVABILITY AND PERFORMANCE METRICS

Observability of a system is the property that determines whether the given states can be uniquely estimated for the system with the available measurements. The metrics used to evaluate the observability of the Fourier coefficients for all the models are outlined in the following sections.

3.1 Observability matrix

The observability matrix of a linearized time-varying system can be constructed from the measurement Jacobian and state-transition matrix (STM). A non-linear time-varying system with constant parameters and no inputs can be described as follows

$$\begin{aligned} \dot{\boldsymbol{x}}(t) &= \boldsymbol{f}(\boldsymbol{x}(t), \boldsymbol{p}), \\ \boldsymbol{y}(t) &= \boldsymbol{h}(\boldsymbol{x}(t), \boldsymbol{p}). \end{aligned} \tag{18}$$

where $\boldsymbol{x}(t) \in \mathbb{R}^{n_x}$ and $\boldsymbol{p} \in \mathbb{R}^{n_p}$. The state and measurement Jacobians of the linearized system are then given by

$$\begin{aligned} \boldsymbol{F}(t) &= \left[\frac{\partial \boldsymbol{f}(t)}{\partial \boldsymbol{x}^T(t)}, \frac{\partial \boldsymbol{f}(t)}{\partial \boldsymbol{p}^T}\right], \\ \tilde{\boldsymbol{H}}(t) &= \left[\frac{\partial \boldsymbol{g}(t)}{\partial \boldsymbol{x}(t)^T}, \frac{\partial \boldsymbol{g}(t)}{\partial \boldsymbol{p}^T}\right] \end{aligned} \tag{19}$$

The STM allows the transformation of the linearized states from one time to another as

$$\boldsymbol{\Phi}(t, t_0) = \begin{bmatrix} \frac{\partial \boldsymbol{x}(t)}{\partial \boldsymbol{x}(t_0)^T} & \frac{\partial \boldsymbol{x}(t)}{\partial \boldsymbol{p}^T} \\ \frac{\partial \boldsymbol{p}}{\partial \boldsymbol{x}(t_0)^T} & \frac{\partial \boldsymbol{p}}{\partial \boldsymbol{p}^T} \end{bmatrix} = \begin{bmatrix} \frac{\partial \boldsymbol{x}(t)}{\partial \boldsymbol{x}(t_0)^T} & \frac{\partial \boldsymbol{x}(t)}{\partial \boldsymbol{p}^T} \\ \boldsymbol{0}_{n_p \times n_x} & \boldsymbol{I}_{n_p \times n_p} \end{bmatrix} \tag{20}$$

It can be computed by numerically integrating the following differential equation [16]

$$\dot{\boldsymbol{\Phi}}(t, t_0) = \boldsymbol{F}(t)\boldsymbol{\Phi}(t, t_0), \qquad \text{with} \qquad \boldsymbol{\Phi}(t_0, t_0) = \boldsymbol{I} \tag{21}$$

The complete measurement sensitivity matrix for the data-arc can then be computed by

$$\boldsymbol{H} = \begin{bmatrix} \tilde{\boldsymbol{H}}(t_0) \\ \tilde{\boldsymbol{H}}(t_1)\boldsymbol{\Phi}(t_1, t_0) \\ \vdots \\ \tilde{\boldsymbol{H}}(t_M)\boldsymbol{\Phi}(t_M, t_0) \end{bmatrix} \tag{22}$$

Finally, the observability matrix can be calculated as

$$\mathscr{O} = \boldsymbol{H}^T\boldsymbol{H} \tag{23}$$

Incorporating the measurement noise and multiplying out the individual matrix blocks, the stochastic observability matrix is given by [7]

$$\mathscr{O} = \sum_{k=1}^{M} \boldsymbol{\Phi}(t_k,t_0)^T \tilde{\boldsymbol{H}}(t_k)^T \boldsymbol{R}^{-1} \tilde{\boldsymbol{H}}(t_k) \boldsymbol{\Phi}(t_k,t_0) \tag{24}$$

Note that the stochastic observability matrix is basically the Fisher information matrix assuming no apriori information. The binary test of observability is carried out by evaluating the rank of the stochastic observability matrix. If the matrix is full-ranked, all the states and parameters are observable. The amount of deficiency in rank indicates the number of unobservable parameters in the system. The numerical evaluation of rank depends on the machine precision and can lead to an incorrect result due to numerical issues. A more accurate method of evaluating the rank is to calculate the singular values. For the matrix to be full-ranked, all the singular values should be above the following threshold [7],

$$s_{\text{threshold}} = \max(s_i) \times \text{size}(\mathscr{O}) \times \text{eps} \tag{25}$$

where $\max(s_i)$ is the largest singular value of the observability matrix, $\text{size}(\mathscr{O})$ is the size of the observability matrix and eps is the machine precision.

3.2 Orthogonalization of the sensitivity matrix

The observability of a parameter for a given system with available measurements is intricately tied to the measurement sensitivity matrix as seen in Eq. 23. In order for the observability matrix to be full-ranked, the sensitivity matrix needs to be full column-ranked. There are two aspects that are to be considered here. First, if the effect of the parameter on the measurements is negligible, then the norm of the sensitivity vector corresponding to that parameter will be nearly zero. Second, if the effect of multiple parameters are indistinguishable, then the corresponding sensitivity vectors are linearly dependent. In both cases, the measurement sensitivity matrix and therefore the observability matrix will be rank-deficient. The rank and singular values of the sensitivity matrix or the observability matrix provide information on the linear dependence between sensitivity vectors but they do not indicate which vectors should be removed from the matrix to improve observability. In fact, even if the linearly dependent vector subset is somehow identified, there's usually a choice on which vectors should be removed from the subset in order to make the rest linearly independent. This choice should be dictated by the norm of the individual sensitivity vectors. Measures such as collinearity index [10] in conjunction with sensitivity norms can be manually used to remove linearly dependent vectors from the sensitivity matrix. This process can be automated by employing an sequential orthogonalization method such as the Gram-Schmidt algorithm [11, 12] outlined as follows. For the given data-arc, the total sensitivity vector corresponding to parameter p_i is given by

$$\boldsymbol{s_i} = \left[\frac{d\boldsymbol{y}(t_0)^T}{dp_i}, \frac{d\boldsymbol{y}(t_1)^T}{dp_i}, \ldots, \frac{d\boldsymbol{y}(t_M)^T}{dp_i} \right]^T \tag{26}$$

This work is concerned only with the observability of the parameters and assumes that all the states are observable. Therefore, the required sensitivity matrix is constructed by concatenating the total sensitivity vectors corresponding to the parameters as follows

$$\mathscr{S} = \boldsymbol{W_1}[\boldsymbol{s_1}, \boldsymbol{s_2}, \ldots, \boldsymbol{s}_{n_p}]\boldsymbol{W_2} = \boldsymbol{W_1 H_p W_2} \tag{27}$$

where $\boldsymbol{H_p}$ is the part of the total measurement matrix given by Eq. 22 corresponding to the parameters, and $\boldsymbol{W_1}$ and $\boldsymbol{W_2}$ are diagonal scaling matrices. With the sensitivity matrix constructed using Eq. 27, the sequential orthogonalization process can be carried out. The basic premise of the method is selecting the vector with the largest norm at the current step and subtracting the projections onto the selected vector from all other vectors. To illustrate, let $\boldsymbol{s_i}$ be the sensitivity vector with the largest norm. Then, parameter i is ranked first. Therefore, $\boldsymbol{q_1} = \dfrac{\boldsymbol{s_i}}{||\boldsymbol{s_i}||}$ is selected as the first vector and the projection of all other vectors onto $\boldsymbol{q_1}$ is removed,

$$\tilde{\boldsymbol{s}}_{\boldsymbol{j}} = \boldsymbol{s_j} - (\boldsymbol{q_1}^T \boldsymbol{s_j})\boldsymbol{q_1}, \qquad j = \{1,2,\ldots,M\} - \{i\} \tag{28}$$

Now, the process is repeated for the new set of vectors with the cardinality decreased by one. Therefore, at each step, the parameter with the largest sensitivity in the direction orthogonal to the previously selected sensitivities is selected until all the parameters have been ranked. This method can be represented in the form of QR decomposition of the sensitivity matrix with column pivoting [13] as $\mathscr{S}E = QR$, where E is the permutation matrix whose columns dictate

the ranks of the parameters, the columns of Q contain the selected directions at each step and R is an upper triangular matrix with columns containing the projections of the sensitivities. A simple example with 3 parameters and 3 outputs helps illustrate the form of the matrices [12, 13]. If the selection order for the sensitivity matrix $\mathscr{S} = [\boldsymbol{s_1}, \boldsymbol{s_2}, \boldsymbol{s_3}]$ is $2, 3, 1$, then the QR decomposition is given by

$$\mathscr{S}\begin{bmatrix} 0 & 1 & 0 \\ 0 & 0 & 1 \\ 1 & 0 & 0 \end{bmatrix} = \begin{bmatrix} \boldsymbol{q_1} & \boldsymbol{q_2} & \boldsymbol{q_3} \end{bmatrix} \begin{bmatrix} \boldsymbol{q_1}^T\boldsymbol{s_2} & \boldsymbol{q_1}^T\boldsymbol{s_3} & \boldsymbol{q_1}^T\boldsymbol{s_1} \\ 0 & \boldsymbol{q_2}^T\boldsymbol{s_3} & \boldsymbol{q_2}^T\boldsymbol{s_1} \\ 0 & 0 & \boldsymbol{q_3}^T\boldsymbol{s_1} \end{bmatrix} \tag{29}$$

Therefore, E contains the ranks of the parameters and the diagonal elements of R contains the orthogonal fractions of the sensitivity vectors. The scaling matrices in Eq. 27 can change the outcome of the method significantly. If $\boldsymbol{W_1}$ is selected to contain the inverse of the measurement noise standard deviation in the diagonal and $\boldsymbol{W_2}$ is the identity matrix, then the sensitivity matrix has a direct relationship with the stochastic observability matrix. But in this case, the ranking assumes that all the nominal parameters have the same value. It is more appropriate to multiply the sensitivities with the possible variation of the parameters, i.e., W_2 contains the initial standard deviations of the parameters in the diagonal. If the sensitivity of the parameters due to the given uncertainty is small, then the parameter should be ranked lower even if the sensitivity due to the nominal value is relatively larger.

The QR orthogonalization method is used to assign ranks to the parameters on the basis of norm and linear dependence between them. In order to determine till what rank the parameters should be estimated, the magnitude of the time dependent relative sensitivity vectors can be used. The relative sensitivity vector is given by

$$\boldsymbol{s_i^r}(t_k) = \boldsymbol{R}^{-1}\frac{d\boldsymbol{y}(t_k)}{dp_i}\boldsymbol{p_i} \tag{30}$$

The norm of the relative sensitivity vector is akin to a 'signal-to-noise ratio (SNR)' for the system. If the norm remains smaller than 1 for the given time-interval, the effect of the parameter on the measurements is smaller than the noise level and can be ignored for the data-arc. This metric can be used as a cut-off for estimating the ranked parameters.

3.3 Consider covariance analysis

A consider covariance analysis ascertains the effect of ignored parameters on the uncertainties of the estimated parameters. Instead of ignoring the non-estimated coefficients, consider covariance analysis recognizes the associated uncertainties and possible errors and quantifies their effects by including their uncertainties in the error covariance matrix. Therefore, considered parameters are assumed to be constant in the estimator and their apriori values and uncertainties are assumed to be known [16]. If the covariance matrix of a batch estimator that ignores the non-estimated parameters is $\boldsymbol{P_x}$, then the covariance of the estimator that considers the same parameters is given by

$$\boldsymbol{P}_{xx} = \boldsymbol{P}_x + \boldsymbol{P}_{xc}\overline{P}_{cc}^{-1}\boldsymbol{P}_{xc}^T \tag{31}$$

where $\overline{P}_{cc}$ is the assumed covariance of the considered parameters $\boldsymbol{c}$ and $\boldsymbol{P}_{xc}$ is the covariance between the estimated states and considered parameters. In order for the non-estimated parameters to be negligible, $\boldsymbol{P}_{xx} \approx \boldsymbol{P}_x$.

3.4 Integrated acceleration error

Consider two time-varying arbitrary states $x(t)$ and $y(t)$ with their derivatives given by $\dot{x}(t)$ and $\dot{y}(t)$. The states at any time are given by

$$\begin{aligned} x(t) &= x_0 + \int_{t_0}^{t} \dot{x}(t)dt \\ y(t) &= y_0 + \int_{t_0}^{t} \dot{y}(t)dt \end{aligned} \tag{32}$$

where x_0 and y_0 are initial states. The error between the two states can be written as

$$(x(t) - y(t)) = (x_0 - y_0) + \int_{t_0}^{t} (\dot{x}(t) - \dot{y}(t))dt \tag{33}$$

The error between the two states is a function of the error between the acceleration integrals. Therefore, even if the RMS of the error between the two accelerations is small, the error in the propagated states can be large if the difference between the integrals of the accelerations is significant. The integrated drag acceleration error is essentially an integral of the drag coefficient error (ΔC_d) weighted by the density ($\rho(t)$), square of the relative velocity ($V_r(t)$) and other constant parameters. Even if the drag coefficient error is smaller for a model, the weighted sum may not be. In other words, $\int_{t_0}^{t} \Delta C_d(t)dt$ being smaller for a model does not imply $\int_{t_0}^{t} \Delta C_d(t)\rho(t)V_r^2(t)dt$ is smaller as well.

4. OBSERVABILITY ANALYSIS RESULTS

To evaluate the observability metrics for the different Fourier models, elliptical satellite orbits are simulated. The simulation parameters are provided in Table 1. An ideal scenario is considered with only the two-body gravitational force and atmospheric drag acting on the satellite for the observability analysis. A spherically symmetric exponentially decaying atmosphere is assumed in the simulations so that non-periodic variations in drag-coefficient can be neglected. A more realistic scenario is considered for the performance metrics. The true drag-coefficient is simulated using the quasi-specular modification of diffuse reflection incomplete accommodation (DRIA) model [19]. A spherical satellite is considered for the OFF model to remove any variations due to attitude. Inertially stabilized symmetrical and asymmetrical cubical satellites are considered for the BFF model.

Position and velocity measurements from a GPS receiver are assumed to be available to the estimator every 10 seconds. The measurements are modeled by adding Gaussian noise with standard deviations of 1.5 m and 0.5 cm/s respectively to the simulated orbital states in the Earth-centered Earth-fixed (ECEF) frame. A nonlinear least-squares batch estimator is used to process the measurements and obtain estimates of position, velocity and the Fourier coefficients. The details are provided in Ray et al [2].

Parameter		Value
Orbital elements	H_p	300 km
	H_a	500 km
	i_0	65^0
	Ω_0	60^0
	ω_0	40^0
Satellite parameters	m	500 kg
	S	10 m^2
Atmospheric parameters	$F_{10.7}$	150 s.f.u
	ρ_0	1.9417e-11 kg/m^3
	H	49.23 km

Table 1: Simulation parameters common for all the cases

4.1 OFF model

For the ideal scenario considered in the simulation, all the sine coefficients are zero for the OFF model. This is because the drag-coefficient is an even function of the eccentric anomaly since the atmosphere is considered to be spherically symmetric. The first step is to determine if all the Fourier coefficients are observable if no prior information is available on them. This can be determined by comparing the singular values of the stochastic observability matrix to the threshold in Eq. 25. The two smallest singular values and the threshold are plotted in Fig. 1. The smallest singular value is above the threshold for some initial duration but then drops below it. Therefore, all the coefficients are not fully observable with the given data-arc.

All the Fourier coefficients are ranked using the QR decomposition method in Fig. 2. The ranking follows the order of the coefficients monotonically. It should be noted that the assigned ranks are highly dependent on the scaling matrices $\boldsymbol{W_1}$ and $\boldsymbol{W_2}$ that have been taken to be the inverse of the measurement noise standard deviations and the initial standard deviations of the Fourier coefficients. It can be seen that only the first four coefficients, until order 3, have an SNR greater than 1. Therefore, the order of coefficients to be estimated should be cut-off at 3.

The effects of ignoring higher-order coefficients on the uncertainty of the estimated states are studied by a consider covariance analysis. At each truncation order of the Fourier series, all the lower-order coefficients are estimated and the higher-order coefficients are considered. The standard deviation norm of position, velocity and the zeroth-order coefficient are plotted in Fig. 3. The solid lines represent the standard deviations obtained by a batch estimator which assumes no uncertainty in the consider parameters and the dashed lines represent the consider standard deviations. It can be seen that in order for the two standard deviations to be consistent for position and velocity each, the Fourier coefficients need to be estimated at least up to order 1. In order for the standard deviations to be consistent for order 0 coefficient, the Fourier coefficients need to be estimated at least to order 2. It is desirable to estimate coefficients to an

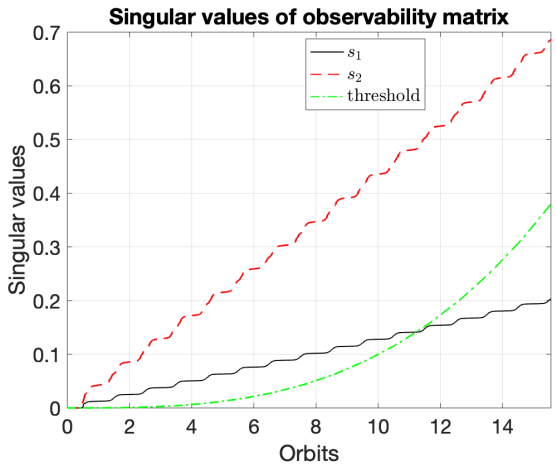

(b)

Fig. 1: OFF model for a spherical satellite: (a) Rank of the stochastic observability matrix; (b) Smallest singular values of the stochastic observability matrix

order higher. Therefore, the Fourier coefficients need to be estimated at least to order 3 which is consistent with the results from the QR decomposition and SNR metrics.

In order to verify the results of the parameter ranking and consider covariance analysis, Monte Carlo simulations are carried out for the cases summarized in Table 2.

Case	**Estimated coefficients**
1	$\overline{\mathbb{A}}_0$
2	$\overline{\mathbb{A}}_0, \overline{\mathbb{A}}_1$
3	$\overline{\mathbb{A}}_0, \overline{\mathbb{A}}_1, \overline{\mathbb{A}}_2$
4	$\overline{\mathbb{A}}_0, \overline{\mathbb{A}}_1, \overline{\mathbb{A}}_2, \overline{\mathbb{A}}_3$
5	$\overline{\mathbb{A}}_0, \overline{\mathbb{A}}_1, \overline{\mathbb{A}}_2, \overline{\mathbb{A}}_3, \overline{\mathbb{A}}_4$
6	$\overline{\mathbb{A}}_0, \overline{\mathbb{A}}_1, \overline{\mathbb{A}}_3$
7	$\overline{\mathbb{A}}_0, \overline{\mathbb{A}}_2, \overline{\mathbb{A}}_3$

Table 2: OFF model for a spherical satellite: Monte Carlo simulation cases

For each case in Table 2, 200 batch estimation runs are performed. The initial state and Fourier coefficient errors are generated from the initial covariance and the measurement noise from the measurement noise covariance for each run. The drag-coefficient is calculated using the estimated Fourier coefficients and the RMS value of the drag-coefficient error is noted. The mean and standard-deviation of the error RMS is plotted for each case in Fig. 4. The figure compares the estimation errors for two scenarios - when the all the non-estimated coefficients are ignored in the filter dynamics versus when they are modeled and kept constant at their nominal values. Note that the errors in the nominal values of the non-estimated coefficients are generated from their nominal covariance for each run. The first thing that can be noticed from Fig. 4 is that the errors are smaller if the non-estimated coefficients are modeled in the estimator for most of the cases. The drag-coefficient errors are equally large for cases 1 and 7, i.e., not estimating $\overline{\mathbb{A}}_1$ results in an inaccurate drag-coefficient estimate. But not estimating any Fourier coefficient other than order 0 results in a large initial position error as well as seen in Fig. 4 (b). If all the coefficients are modeled, then estimating coefficients after order 2 does not add further accuracy to the overall drag-coefficient whereas the order goes up to 3 if the non-estimated coefficients are ignored. Overall, the results indicate that the all the coefficients up to order 2 should be estimated with all the higher-coefficients being modeled.

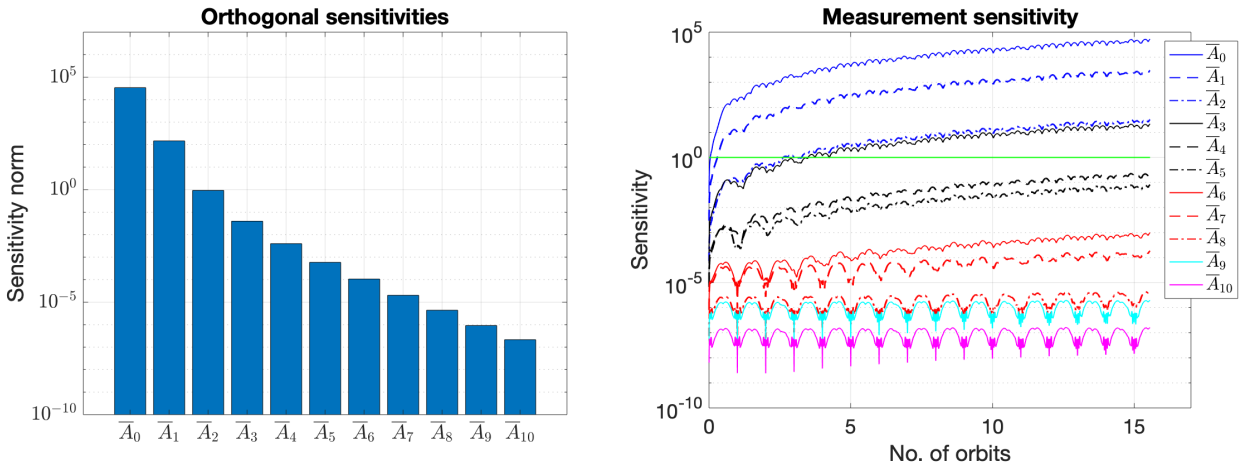

(a) (b)

Fig. 2: OFF model for a spherical satellite: (a) Norm of the orthogonal fractions of the total normalized sensitivity vectors; (b) Norm of the time-varying relative sensitivity vectors

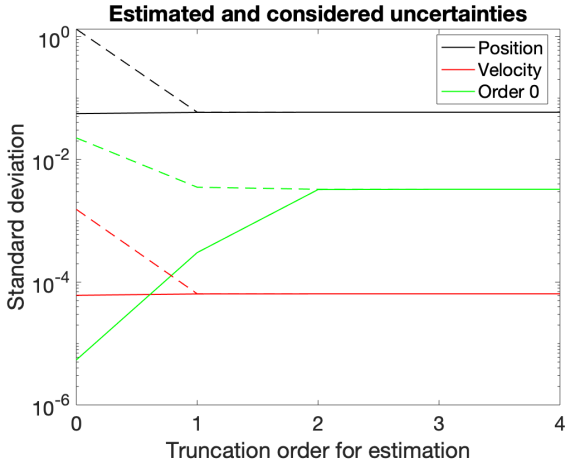

Fig. 3: OFF model for a spherical satellite: Standard deviations assuming no errors in consider parameters (solid lines) and consider standard deviations (dashed lines) for position, velocity and zeroth-order Fourier coefficient

4.2 BFF/BODF model

Unlike the OFF coefficients, the BFF coefficients are tied to the body frame and capture variations in the drag-coefficient due to attitude. The OFF coefficients are slowly varying if there are no variations in the attitude of the satellite and can therefore be considered constant in the orbit determination process. But the BFF coefficients will have variations in the orbit due to ambient parameters. Since the coefficients are estimated as constants in the estimator, there will be a certain degree of mismatch between the true and filter dynamics. But this mismatch can be reduced by modeling and/or estimating the BODF coefficients along with the BFF coefficients. In this section, the BFF and BODF coefficients are estimated for a satellite with an inertially stabilized profile. For the simulations, a box-wing shape model for the satellite is considered. Two solar panels with an area of 13.5 m^2 each are fixed to the satellite bus [2]. The dimensions of the satellite bus are taken to be 1.5x2x2.5 m^3. The body z-axis is perpendicular to the solar panels and the y-axis is parallel to solar panel axis. Additional areas of 1, 0.75, 1.5, 1, 1.5, 0.1 m^2 are added to the faces in +x, -x, +y, -y, +z and -z directions to take into account asymmetry due to shape details such as protrusions etc. The surface material properties are considered to be different for each panel. The total number of non-zero coefficients for this case is 118 and the observability matrix is highly rank-deficient.

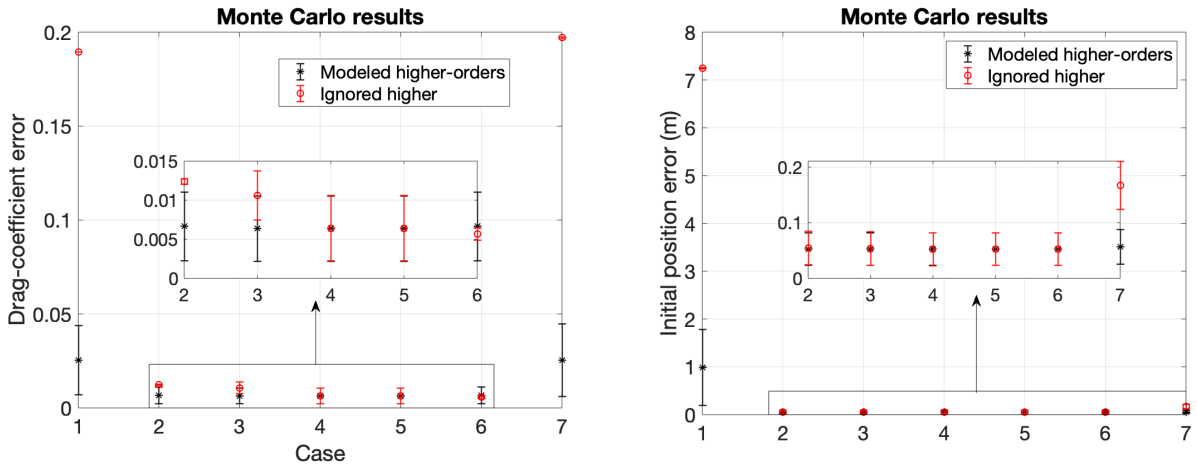

(a) (b)

Fig. 4: OFF model for a spherical satellite: Mean and 1σ error bars for (a) Drag-coefficient error RMS values; (b) Norm of initial position error for the Monte Carlo cases

The non-dimensionalized sensitivity norm of all the coefficients with an SNR greater than 1 are plotted in Fig. 5 (b). The rank of first few coefficients are plotted in Fig. 5 (a). It can be seen that after $\overline{\mathbb{A}}_{0,1}$, coefficients with SNR $<$ 1 start getting ranked higher than coefficients with SNR $>$ 1. Therefore, it is reasonable to assume that coefficients ranked lower than $\overline{\mathbb{A}}_{0,1}$ may not need to be estimated. But some of the lower ranked coefficients with SNR $>$ 1 are still included in subsequent analysis.

A consider covariance analysis with estimation subsets given by Table 3 shows that it is sufficient to estimate the ranked coefficients until $\overline{\mathbb{A}}_{0,1}$. This is verified through a Monte Carlo analysis with the same cases. Figs. 7 and 8 shows that a significant reduction in the drag-coefficient error as well as initial position error is achieved from case 4 to case 5. The measurement residual ratio is also slightly closer to 1 for case 5.

Since the body and orbit angles vary at similar rates for an inertially stabilized satellite, it is possible that even though the drag-coefficient accuracy is improved for the BODF model, the individual Fourier coefficients might have larger errors due to aliasing effects. But the estimation errors for the coefficients in Table 4 prove that the Fourier coefficients have a higher accuracy when they are estimated versus when they are not. Therefore, the overall improvement in the drag-coefficient is due to the improvement in the estimation accuracy of the Fourier coefficients.

Case	Estimated coefficients
1	$\overline{\mathbb{A}}_{0,0}$
2	$\overline{\mathbb{A}}_{0,0}, \overline{\mathbb{A}}_{2,0}$
3	$\overline{\mathbb{A}}_{0,0}, \overline{\mathbb{A}}_{2,0}, \overline{\mathbb{B}}_{1,0}$
4	$\overline{\mathbb{A}}_{0,0}, \overline{\mathbb{A}}_{2,0}, \overline{\mathbb{B}}_{1,0}, \overline{\mathbb{A}}_{4,0}$
5	$\overline{\mathbb{A}}_{0,0}, \overline{\mathbb{A}}_{2,0}, \overline{\mathbb{B}}_{1,0}, \overline{\mathbb{A}}_{4,0}, \overline{\mathbb{A}}_{0,1}$
6	$\overline{\mathbb{A}}_{0,0}, \overline{\mathbb{A}}_{2,0}, \overline{\mathbb{B}}_{1,0}, \overline{\mathbb{A}}_{4,0}, \overline{\mathbb{A}}_{0,1}, \overline{\mathbb{A}}_{6,0}$
7	$\overline{\mathbb{A}}_{0,0}, \overline{\mathbb{A}}_{2,0}, \overline{\mathbb{A}}_{1,0}, \overline{\mathbb{A}}_{4,0}, \overline{\mathbb{A}}_{0,1}, \overline{\mathbb{A}}_{6,0}, \overline{\mathbb{A}}_{2,1}$
8	$\overline{\mathbb{A}}_{0,0}, \overline{\mathbb{A}}_{2,0}, \overline{\mathbb{A}}_{1,0}, \overline{\mathbb{A}}_{4,0}, \overline{\mathbb{A}}_{0,1}, \overline{\mathbb{A}}_{6,0}, \overline{\mathbb{A}}_{2,1}, \overline{\mathbb{B}}_{1,1}$
9	$\overline{\mathbb{A}}_{0,0}, \overline{\mathbb{A}}_{2,0}, \overline{\mathbb{A}}_{1,0}, \overline{\mathbb{A}}_{4,0}, \overline{\mathbb{A}}_{0,1}, \overline{\mathbb{A}}_{6,0}, \overline{\mathbb{A}}_{2,1}, \overline{\mathbb{B}}_{1,1}, \overline{\mathbb{A}}_{2,3}$

Table 3: Monte Carlo simulation cases for BODF model for an asymmetrical satellite

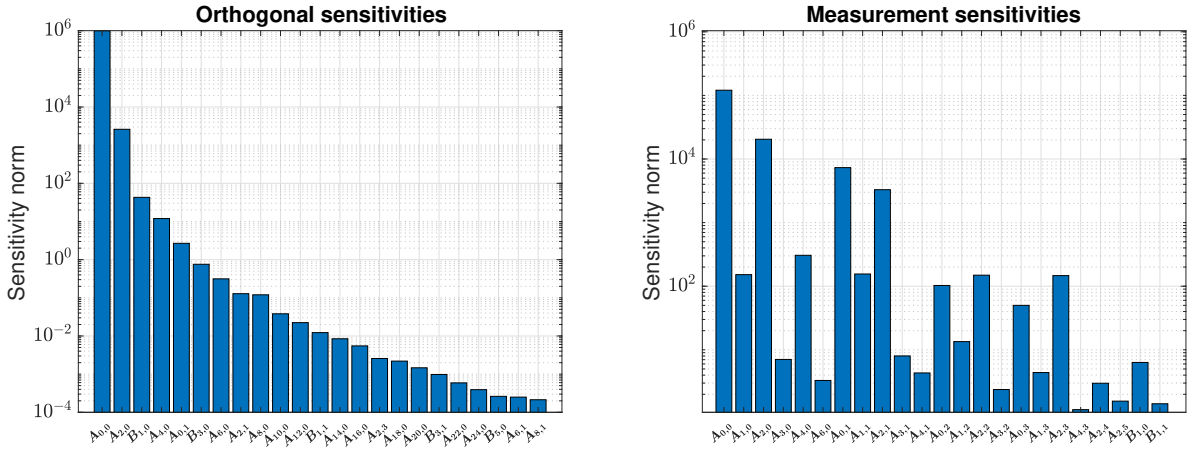

(a) (b)

Fig. 5: BODF results for an asymmetrical satellite: (a) Norm of the orthogonal fractions of the total normalized sensitivity vectors; (b) Norm of the time-varying relative sensitivity vectors for a symmetrical cube for Monte Carlo cases

5. ORBIT PREDICTION RESULTS

The previous section discussed the dependence of orbit determination results on observability of the coefficients in idealized scenarios. This section extends the analysis to the prediction regime in more realistic scenarios and demonstrates a better orbit determination fit in terms of traditional performance metrics may not imply a better prediction performance. The forces considered for the true trajectory and the filter model are given in Table 5. In order to compare the prediction performance of the higher-order Fourier models with order 0 (standard cannonball) model, the in-track errors of the predicted orbits are plotted in Fig. 9 for an inertially stabilized attitude profile.

All the higher orders perform better than the standard cannonball model (order 0). Order 2 BODF performs the best, resulting in almost a 90 % improvement in the in-track prediction error over cannonball. In order to understand the relative performances of the models, it is useful to look at the error statistics of the estimated states for the different models. Table 6 lists the RMS values of the post-fit residuals in the radial-tangential-normal (RTN) frame, the norm of the initial errors in the estimated states and the RMS values of the drag coefficient errors. As can be seen from Table 6, the overall prediction errors are an interplay between improvements in orbit fit, estimated SRP coefficient and effective drag coefficient. Even though the OFF model provides the best estimates of the initial position and velocity, better estimates of the drag coefficient are obtained using the other models.

Coefficient	**Estimation error (Case 1)**	**Estimation error (Case 6)**
$\overline{\mathbb{A}}_{0,0}$	0.112	0.011
$\overline{\mathbb{A}}_{2,0}$	0.352	0.034
$\overline{\mathbb{B}}_{1,0}$	0.003	4.079e-4
$\overline{\mathbb{A}}_{4,0}$	0.070	0.036
$\overline{\mathbb{A}}_{0,1}$	0.063	0.027
$\overline{\mathbb{A}}_{6,0}$	0.0234	0.0228

Table 4: Estimation error in the BODF coefficients for an asymmetrical satellite

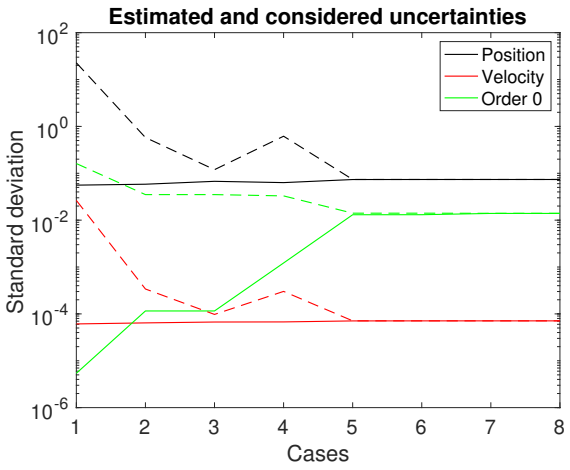

Fig. 6: Standard deviations assuming no errors in consider parameters (solid lines) and consider standard deviations (dashed lines) for position, velocity and zeroth-order Fourier coefficient

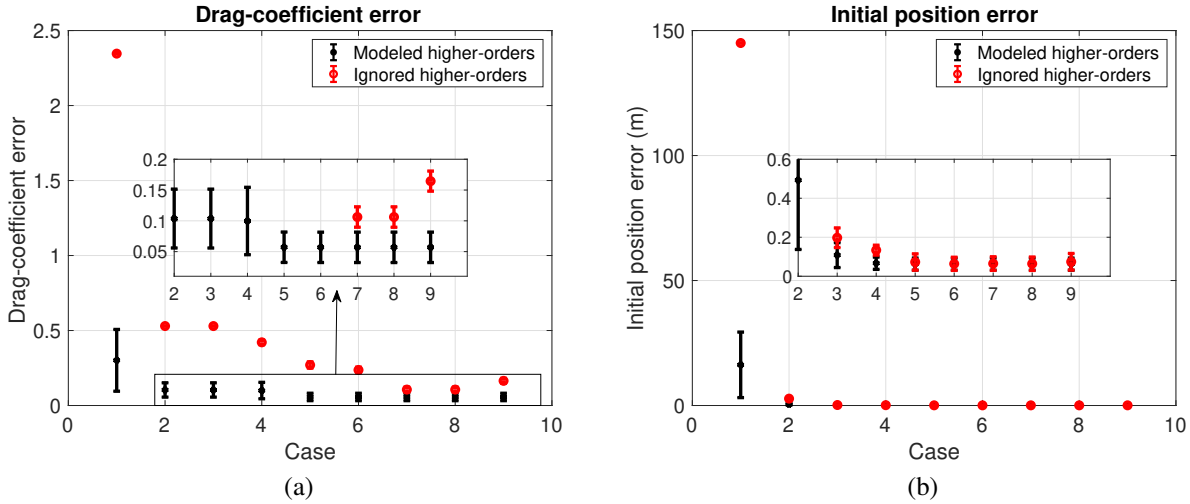

Fig. 7: BODF results for an asymmetrical satellite: Mean and 1σ error bars for (a) Drag-coefficient error RMS values; (b) Norm of initial position error for Monte Carlo cases

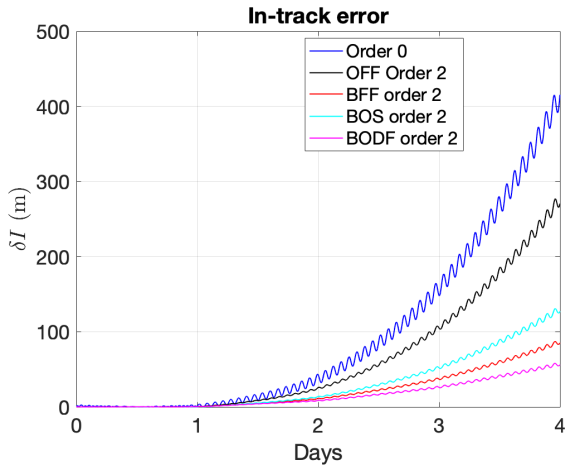

Fig. 9: In-track error for an inertially stabilized satellite. The estimation window is until the end of the first day and the rest is prediction.

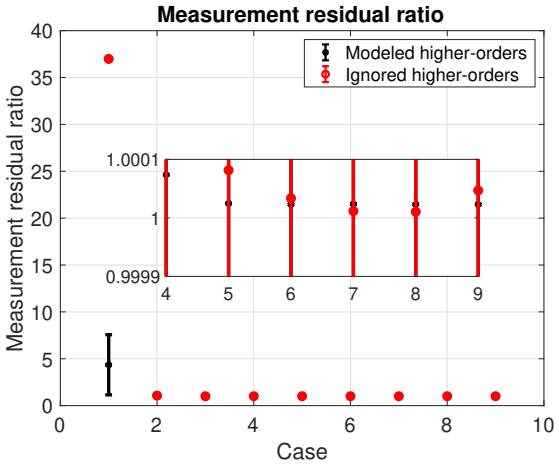

(c)

Fig. 8: BODF results for an asymmetrical satellite: Non-dimensionalized measurement residual RMS values for asymmetrical satellite for Monte Carlo cases

Force	Parameter	True dynamics	Filter dynamics
Geopotential	Order and degree	10x10	10x10
Third-body forces of Sun and Moon	Ephemerides	JPL DE- 430	JPL DE-430
SRP	Model	Panel method	Cannonball, C_r is estimated
Atmospheric drag	Density model	NRLMSISE-00	NRLMSISE-00
	Drag coefficient	GSIM	Fourier model, Coefficients are estimated
	Winds	HWM-07	None
	Attitude noise	None	$\mathcal{N}(0, 0.1^0)$

Table 5: Force models for truth and filter dynamics

Order 2 BOS still performs worse than BFF and BODF even though the error in the initial state estimates and the RMS of drag-coefficient error is smaller for BOS (not presented here for the sake of brevity). Why should the BOS perform worse when the overall errors in the drag acceleration are smaller for the model? The answer lies in the integrated acceleration error. As discussed before, the even when the drag coefficient error may be better, the integrated acceleration error is what decides the final prediction performance. The integrated drag acceleration error for BOS is 7.65×10^{-4} m/s compared to 7.16×10^{-4} m/s for BFF and 5.49×10^{-4} m/s for BODF which explains the worse prediction of BOS even with more accurate orbit determination metrics.

6. CONCLUSIONS

Observability analysis using various metrics such as ranking of Fourier coefficients based on QR orthogonalization, non-dimensionalized measurement sensitivity, correlation coefficients and consider covariances was undertaken for the Fourier drag-coefficient models. These observability analysis results were directly compared with orbit determination fits through Monte Carlo simulations. Using parameter ranking based on QR orthogonalization and the ratio of measurement sensitivity to measurement noise standard deviation facilitates the selection of estimation subset. A

Parameter		Error RMS/Norm				
		Order 0	**OFF**	**BFF**	**BOS**	**BODF**
Post-fit residuals (m)	R	1.5804	1.5044	1.5041	1.5040	**1.5039**
	T	1.7929	1.5148	1.5110	1.5106	**1.5096**
	N	1.4996	1.4995	1.4995	1.4995	1.4995
Initial error	Position (m)	1.260	**0.046**	0.134	0.152	0.201
	Velocity (m)	8.994e-4	**4.804e-5**	1.347e-4	1.670e-4	2.303e-4
	C_r	1.15	0.13	0.19	**0.01**	0.03
Drag coefficient	Total	1.11	0.91	0.86	**0.84**	0.88

Table 6: RMS and norm of errors for inertially stabilized satellite. The smallest values for each parameter are highlighted

consider covariance analysis performed in conjunction allows a verification that the selected coefficients have the dominant effect on filter uncertainties. In every case, the set selected through the observability analysis leads to the best orbit-determination fit in terms of overall drag-coefficient error, initial position error and post-fit residuals. For all the drag-coefficient models, less than six coefficients need to be estimated and rest of the coefficients modeled to obtain the best orbit-fit achievable. Through the introduction of a new metric, integrated acceleration error, it was demonstrated that a better orbit-fit in terms of traditional metrics such as post-fit residuals does not guarantee a better prediction performance. But the integrated acceleration error cannot be calculated for actual orbit-determination scenarios since the true trajectory will not be known. A new metric is required such that the orbit prediction performance of proposed models can be appropriately correlated with the orbit-determination performance.

7. REFERENCES

[1] D.M. Lucchesi. Reassessment of the Error Modelling of Nongravitational Perturbations on LAGEOS II and Their Impact in the Lense-Thirring Determination. Part I. *Planetary and Space Science*, 49:447–463, 2001.

[2] Vishal Ray, Daniel J. Scheeres, Siamak G. Hesar, and Matthew Duncan. A drag coefficient modeling approach using spatial and temporal Fourier expansions for orbit determination. *Journal of the Astronautical Sciences*, 2019.

[3] Vishal Ray and Daniel J. Scheeres. A drag coefficient model to track variations due to attitude and orbital motion. *Journal of Guidance, Control and Dynamics (in production)*, 2020.

[4] Z. Chen. Local observability and its application to multiple measurement estimation. *IEEE Trans. Ind. Electron.*, 38(6):491–496, 1991.

[5] Bruce P. Gibbs. *Advanced Kalman Filtering, Least-Squares and Modeling*. John Wiley & Sons, 2011.

[6] A.J. Krener and K. Ide. Measures of unobservability. In *Proceedings of the 48th IEEE Conference on Decision and Control, 2009 Held Jointly with the 2009 28th Chinese Control Conference*, pages 6401–6406.

[7] Alex M. Friedman and Carolin Frueh. Determining characteristics of artificial near-Earth objects using observability analysis. *Acta Astronautica*, 144:405–421, 2018.

[8] Jeroen L. Geeraert. *Multi-Satellite Orbit Determination Using Interferometric Observables with RF Localization Applications*. PhD thesis, University of Colorado Boulder, 2017.

[9] Siamak G. Hesar. *A Framework for Precise Orbit Determination of Small Body Orbiting Spacecraft*. PhD thesis, University of Colorado Boulder, 2016.

[10] Roland Brun, Peter Reichert, and R. Hans Künsch. Practical identifiability analysis of large environmental simulation models. *Water Resources Research*, 37(4):1015–1030, 2001.

[11] Yunfei Chu and Juergen Hahn. Generalization of a Parameter Set Selection Procedure Based on Orthogonal Projections and the D-Optimality Criterion. *Process Systems Engineering*, 58(7):2085–2096, 2012.

[12] Berit Floor Lund and Bjarne A. Foss. Parameter ranking by orthogonalization—Applied to nonlinear mechanistic models. *Automatica*, 44:278–281, 2008.

[13] Berit Floor Lund, Hans E. Berntsen, and Bjarne A. Foss. Methods for Parameter Ranking in Nonlinear, Mechanistic Models. In *IFAC Proceedings Volumes*, volume 28, pages 578–583, 2005.

[14] L. Fraiture. The information dilution theorem. *ESA Journal*, 10(4):381–386, 1986.

[15] Vishal Ray and Daniel J. Scheeres. Gravitational Force-Model Aliasing with Non-Gravitational Force Coefficients in Dynamic Prediction. *Journal of Guidance, Control and Dynamics (in production)*, 2020.
[16] Byron D. Tapley, Bob E. Schutz, and George H. Born. *Statistical Orbit Determination*, chapter 6. Elsevier Academic Press, 2004.
[17] G.A. Bird. *Molecular Gas Dynamics and Direct Simulation of Gas Flows*. Clarendon Press, 1994.
[18] Eelco Doornbos. *Thermospheric Density and Wind Determination from Satellite Dynamics*. PhD thesis, Delft University of Technology, 2011.
[19] Andrew Walker, Piyush Mehta, and Joseph Koller. Drag Coefficient Model Using the Cercignani–Lampis–Lord Gas–Surface Interaction Model. *Journal of Spacecraft and Rockets*, 51(5):1544–1563, 2014.